

# Global coupled-channel analysis of $e^+e^- \rightarrow c\bar{c}$ processes in $\sqrt{s} = 3.75 - 4.7$ GeV

S.X. Nakamura,<sup>1,2,3,\*</sup> X.-H. Li,<sup>2,3</sup> H.-P. Peng,<sup>2,3</sup> Z.-T. Sun,<sup>1</sup> and X.-R. Zhou<sup>2,3</sup>

<sup>1</sup>*Institute of Frontier and Interdisciplinary Science,  
Shandong University, Qingdao, Shandong 266237, China*

<sup>2</sup>*University of Science and Technology of China, Hefei 230026, China*

<sup>3</sup>*State Key Laboratory of Particle Detection and Electronics, Beijing 100049, Hefei 230026, China*

Recent high-precision  $e^+e^- \rightarrow c\bar{c}$  data from the BESIII and Belle are highly useful to understand the vector charmonium pole structure and puzzling lineshapes due to the exotic hadron candidates  $Y$ . We thus conduct a global coupled-channel analysis of most of the available data (9 two-body, 9 three-body, and 1 four-body final states) in  $\sqrt{s} = 3.75 - 4.7$  GeV. Not only cross sections but also invariant mass distributions of subsystems are fitted. Our model includes dozens of (quasi) two-body states that nonperturbatively couple with each other through bare charmonium excitations and particle-exchange mechanisms required by the three-body unitarity. The amplitudes obtained from the fits are analytically continued to vector charmonium and  $Z_c$  poles. We do not find a  $\psi(4160)$  pole that has been considered well-established. Instead, we find two poles of  $\sim 4230$  MeV;  $\psi(4230)$  with  $\Gamma = 36$  MeV and a broader one with  $\Gamma = 114$  MeV. Two  $Z_c$  poles are found as virtual states  $\sim 40$  MeV below the  $D^*\bar{D}^{(*)}$  thresholds, being consistent with lattice QCD results. This work presents the first global analysis to determine the vector charmonium and  $Z_c$  poles, thereby paving the way to extracting detailed properties of the prominent exotic hadron candidates from data.

*Introduction.*— The  $Y$ -sector of  $XYZ$  exotic hadrons was opened with the discovery of  $Y(4260)$  by the BABAR Collaboration [1] in  $e^+e^- \rightarrow \gamma_{\text{ISR}}\pi^+\pi^-J/\psi$  ( $\gamma_{\text{ISR}}$ : initial state radiation  $\gamma$ ), and subsequent confirmations by the CLEO and Belle Collaborations [2, 3].<sup>1</sup> The  $Y(4260)$  structure has been considered exotic for its peculiar decay patterns and not having a quark-model counterpart. The discovery of  $Y$  continued:  $Y(4360)$  in  $e^+e^- \rightarrow \gamma_{\text{ISR}}\pi^+\pi^-\psi'$  by the BABAR [5] and Belle [6], and  $Y(4660)$  by the Belle [6]. The exotic hadrons are considered a key to deepening our understanding of QCD and thus invited lots of studies; see reviews [7–14].

The BESIII pursued the precision frontier of the  $Y$  sector with direct  $Y$  productions without  $\gamma_{\text{ISR}}$ , and found that  $Y$  widths appear differently in their different decay modes ( $Y$ -width problem) [15–23]; see Fig. 4 of [23]. The BESIII also found that  $Y(4260)$  in  $e^+e^- \rightarrow \pi^+\pi^-J/\psi$  consists of  $Y(4220)$  and  $Y(4320)$  [24], and that  $Y(4320)$  does not appear in other final states.  $Y(4360)$  and  $Y(4660)$  were confirmed with higher precision [19, 25].

The  $Y$ -width problem actually indicates no simple relation between resonance parameters from different models fitted to different processes. To solve the  $Y$ -width problem, therefore, different final states need to be analyzed simultaneously with a unified coupled-channel model. This reveals how various charmonia interfere and kinematical effects such as threshold opening/cusp and triangle singularity (TS) work, thereby creating the process-dependent  $Y$  lineshapes.

The  $Z_c^+(3900)$  is also an outstanding exotic  $c\bar{c}u\bar{d}$  candidate, discovered in the  $J/\psi\pi^+$  invariant mass distribution of  $e^+e^- \rightarrow \pi^+\pi^-J/\psi$  [26, 27]. The discovery of

$Z_c^+(4020)$  followed in a study of  $e^+e^- \rightarrow \pi^+\pi^-h_c$  [28]. The properties of  $Z_c$  and  $Y$  should be correlated since  $Z_c$  appear as  $Y \rightarrow Z_c\pi$ . Inevitably, the above coupled-channel analysis considers the  $Z_c$  signals in the data, and addresses their nature.

Regarding previous coupled-channel studies, Cleven et al. [29] fitted  $e^+e^- \rightarrow J/\psi\pi^+\pi^-$ ,  $h_c\pi^+\pi^-$ , and  $DD^*\pi$  cross sections and lineshapes to study  $Y(4260)$ . Detten et al. [30] recently reported a similar study including more final states. Chen et al. [31] and Zhou et al. [32] fitted cross sections of 3–4 processes to explore the  $Y$  poles. Considering the recent data below, the previous analyses used rather limited dataset, which would question the reliability of their conclusions.

In the last several years, the BESIII has accumulated high quality data for various  $e^+e^- \rightarrow c\bar{c}$  cross sections and their invariant mass distributions over a wide energy region [15–25, 33–43]; see Figs. 2 and 3. It is timely to analyze these data simultaneously with a coupled-channel framework, and extract vector charmonium properties such as their poles (mass, width) and residues (branchings). These resonance properties are a primary basis to study the nature of  $Y$  and a prerequisite to answer the  $Y$ -width problem. They are also new information for well-established charmonia [ $\psi(4040)$ ,  $\psi(4160)$ ,  $\psi(4415)$ ] since their properties have been mainly from the inclusive ( $e^+e^- \rightarrow$  hadrons)  $R$  value [44].

In this work, we conduct such a global coupled-channel analysis over  $\sqrt{s} = 3.75 - 4.7$  GeV for the first time, and present the fit results and the vector charmonium and  $Z_c$  pole positions. A full account of this work, including more detailed properties of the charmonia, will be given subsequently [45].

*Model.*— We sketch our coupled-channel model [46–48] for  $e^+e^- \rightarrow c\bar{c}$  processes. For three-body ( $abc$ ) final

<sup>1</sup> While we basically follow the particle name convention of Ref. [4], we also use historical names such as  $Y$ .

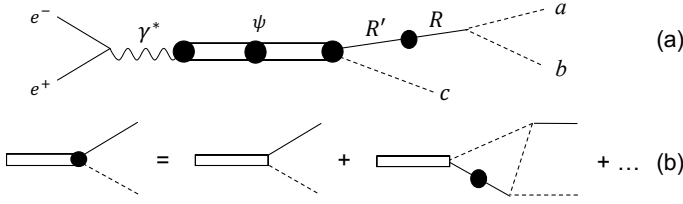


FIG. 1. (a) Charmonium excitation mechanism for  $e^+e^- \rightarrow abc$ ; the solid lines are (bare) two-meson resonances  $R$ . The double lines represent bare charmonium states. The solid circles represent dressed propagators and vertices. (b) Charmonium decays via direct and single triangle mechanisms.

states, a charmonium ( $\psi$ ) excitation amplitude [Fig. 1(a)] is <sup>2</sup>

$$A_{abc,e^+e^-}^\psi = \sum_{abc}^{\text{cyclic}} \sum_{RR's_R^z} \sum_{ij s_\psi^z} \Gamma_{ab,R} \tau_{R,R'}(p_c, E - E_c) \times \bar{\Gamma}_{cR',\psi_i}(\mathbf{p}_c, E) \bar{G}_{ij}(E) \bar{\Gamma}_{\psi_j,e^+e^-}(E), \quad (1)$$

where  $R$  is a two-meson resonance such as  $D_1(2420)$ ; cyclic permutations  $(abc), (cab), (bca)$  are indicated by  $\sum_{abc}^{\text{cyclic}}$ ;  $\psi_i$  indicates  $i$ -th bare  $\psi$  state;  $E$  denotes the  $abc$  invariant mass. The amplitude includes dressed  $\psi$  production mechanism ( $\bar{\Gamma}_{\psi,e^+e^-}$ ), dressed  $\psi$  propagator ( $\bar{G}_{ij}$ ), dressed  $\psi \rightarrow Rc$  vertex ( $\bar{\Gamma}_{cR,\psi}$ ), dressed  $R$  propagator ( $\tau_{R,R'}$ ), and  $R \rightarrow ab$  vertex ( $\Gamma_{ab,R}$ ). We also consider nonresonant (NR) mechanism:

$$A_{abc,e^+e^-}^{\text{NR}} = \sum_{abc}^{\text{cyclic}} \sum_{RR's_R^z} \Gamma_{ab,R} \tau_{R,R'} \bar{\Gamma}_{R',e^+e^-}(\mathbf{p}_c, E) \quad (2)$$

with a NR dressed  $Rc$  production mechanism ( $\bar{\Gamma}_{Rc,e^+e^-}$ ). Amplitudes for two-body final states are obtained from Eqs. (1) and (2) by removing  $\Gamma_{ab,R}\tau_{R,R'}$ . The dressed  $Rc$  propagator is given by

$$[\tau^{-1}(p, E)]_{R,R'} = [E - E_R(p)]\delta_{R,R'} - [\Sigma(p, E)]_{R,R'} \quad (3)$$

with  $\Sigma_{R,R'}$  being the  $R$  self-energy generated by  $\Gamma_{ab,R}$ . The dressed  $\psi \rightarrow Rc$  vertex is given as

$$\bar{\Gamma}_{cR,\psi_i}(\mathbf{p}_c, E) = \int d^3q \Phi_{cR,c'R'}(\mathbf{p}_c, \mathbf{q}; E) \Gamma_{c'R',\psi_i}(\mathbf{q}) \quad (4)$$

with  $\Gamma_{cR,\psi_i}$  being a bare  $\psi_i \rightarrow Rc$  vertex and  $\sum_{c'R's_R^z}$  implicit.  $\Phi = (1 - \int d^3q V\tau)^{-1}$  is a wave function driven

<sup>2</sup> We denote a particle  $x$ 's mass, momentum, energy, and spin state in the  $abc$  center-of-mass (CM) frame by  $m_x, \mathbf{p}_x, E_x$ , and  $s_x^z$ , respectively;  $E_x = \sqrt{m_x^2 + |\mathbf{p}_x|^2}$ . The mass values are from Ref. [4]. Our model is isospin symmetric, and the averaged mass is used for isospin partners.

(a) TABLE I. Quasi two-body ( $Rc$ ) coupled-channels. See text for grouping (A-C).

(A)	$D_1(2420)\bar{D}^{(*)}, D_1(2430)\bar{D}^{(*)}, D_2^*(2460)\bar{D}^{(*)}, D^{(*)}\bar{D}^{(*)}$
(B)	$D_0^*(2300)\bar{D}^*, f_0J/\psi, f_2J/\psi, f_0\psi', f_0h_c, Z_c\pi, Z_{cs}\bar{K}$
(C)	$D_s^{(*)}\bar{D}_s^{(*)}, J/\psi\eta, J/\psi\eta', \omega\chi_{c0}$

by an  $Rc \rightarrow R'c'$  Z-shape interaction  $V$  where  $R \rightarrow c'\bar{c}$  is followed by  $\bar{c}c \rightarrow R'$  via a potentially on-shell  $\bar{c}$ -exchange; see Appendix C of [46] for formulas. This nonperturbative treatment of  $V\tau$  is required by the three-body unitarity, although our model is not fully three-body unitary for partly using BW amplitudes in Eq. (3) as discussed below. Similarly,  $\bar{\Gamma}_{Rc,e^+e^-}$  in Eq. (2) is obtained by replacing  $\Gamma_{c'R',\psi_i}$  in Eq. (4) with a tree  $e^+e^- \rightarrow \gamma^* \rightarrow R'c'$  amplitude ( $\Gamma_{c'R',e^+e^-}$ ). The dressed  $\psi$  production mechanism  $\bar{\Gamma}_{\psi_i,e^+e^-}$  is given by

$$\Gamma_{\psi_i,e^+e^-} + \sum_{cRR's_R^z} \int d^3q \Gamma_{\psi_i,cR'}(\mathbf{q})\tau_{R',R}\bar{\Gamma}_{Rc,e^+e^-}(\mathbf{q}, E), \quad (5)$$

where the first term is a bare  $e^+e^- \rightarrow \gamma^* \rightarrow \psi_i$  amplitude and the second rescattering term. The dressed  $\psi$  propagator is

$$[\bar{G}^{-1}(E)]_{ij} = (E - m_{\psi_i})\delta_{ij} - [\Sigma_\psi(E)]_{ij}, \quad (6)$$

with a bare mass  $m_{\psi_i}$  and the self energy

$$[\Sigma_\psi(E)]_{ij} = \sum_{cRR's_R^z} \int d^3q \Gamma_{cR,\psi_i}(\mathbf{q})\tau_{R,R'}\bar{\Gamma}_{cR',\psi_j}(\mathbf{q}, E). \quad (7)$$

We consider  $Rc$  channels summarized in Table I. Each channel is combined with its charge conjugate to form a negative  $C$ -parity state. For the group (A), we simplify Eq. (3) to a BW form with mass and width (constant) from [4]. Their decay vertices  $\Gamma_{ab,R}$  are determined, assuming that  $D_1(2420) \rightarrow D^*\pi$  (mainly  $d$ -wave),  $D_1(2430) \rightarrow D^*\pi$  ( $s$ -wave),  $D_2^*(2460) \rightarrow D^*\pi + D\pi$  [ $\Gamma(D\pi)/\Gamma(D^*\pi) \sim 1.5$  [4]], and  $D^* \rightarrow D\pi$  saturate their widths. A small  $s$ -wave decay of  $D_1(2420)$  is also included to reproduce the helicity angle distribution [54]. Regarding the group (B),  $R$  is pole(s) from meson-meson scattering driven by bare  $\Gamma_{ab,R}$ .  $D_0^*(2300)$  is from  $D\pi$   $s$ -wave scattering amplitude fitted to that based on the lattice QCD spectrum [55].  $f_0$  and  $f_2$  are poles from  $s$ - and  $d$ -wave  $\pi\pi - K\bar{K}$  coupled-channel amplitudes, respectively [56].  $Z_c$  represents poles from a  $J^{PC} = 1^{+-} D^*\bar{D} - D^*D^* - J/\psi\pi - \psi'\pi - h_c\pi - \eta_{c\rho}$  coupled-channel scattering amplitude ( $Z_c$  amplitude).  $Z_{cs}$  is introduced to simply provide a  $\psi_i \rightarrow J/\psi K\bar{K}$  mechanism and no pole. The group (C) channels are treated stable;  $\Sigma_{RR'} = 0$  in Eq. (3). See the Supplemental Material for more on the model and cross section formulas.

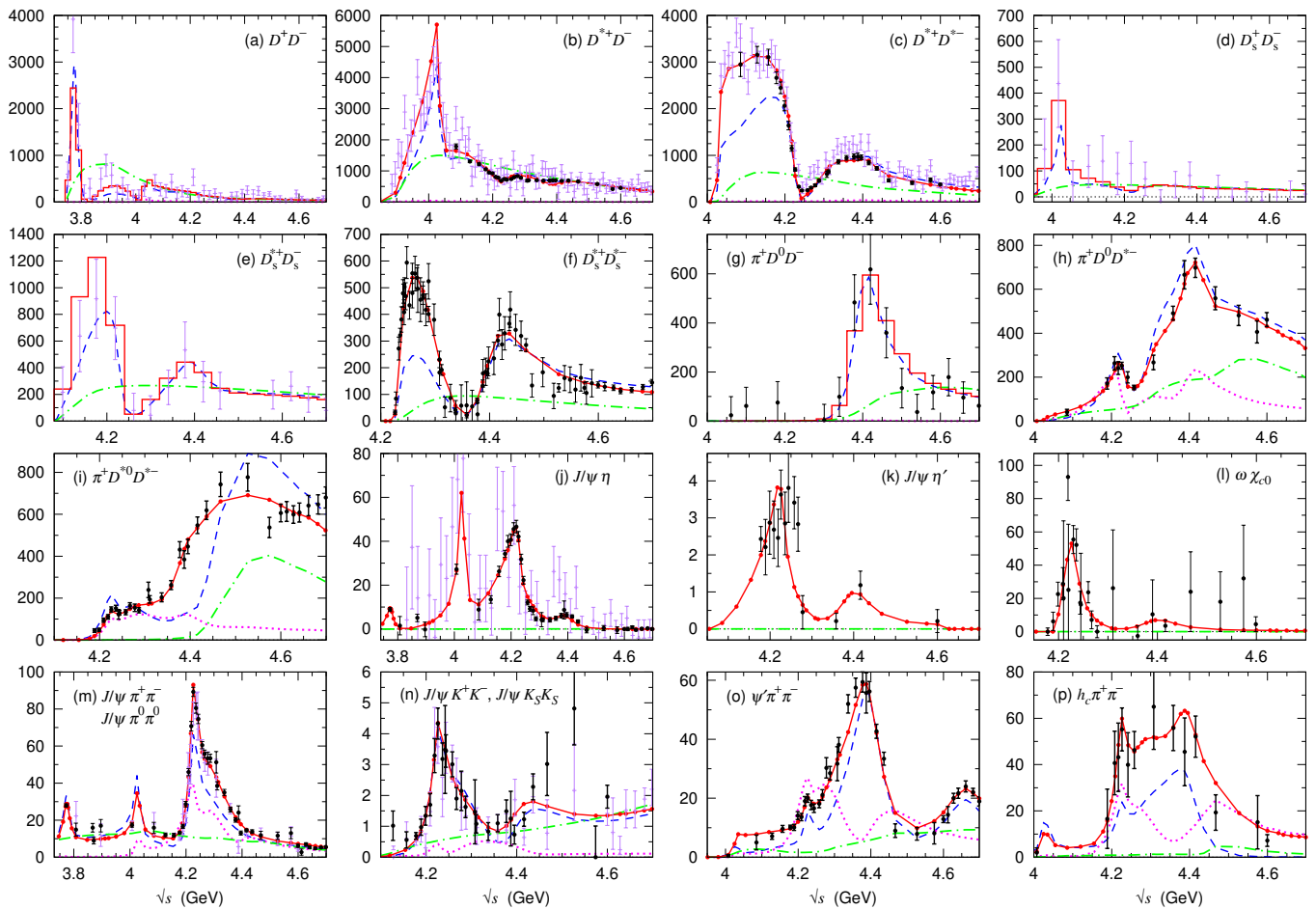


FIG. 2. Cross sections (unit:pb) for  $e^+e^-$  annihilations into various final states (indicated in each panel) as functions of the total energy  $\sqrt{s}$ . The red points are from our coupled-channel calculation; the lines are just for guiding eyes. The blue dashed, magenta dotted, and green dash-dotted curves are the direct decays, one-loop, and nonresonant contributions, respectively. To compare with initial-state radiation data (a,d,e,g), the calculated cross sections have been averaged within each bin. The data are from Ref. [49] in the panel (a); [33] (black) and [50] (purple) in (b) and (c); [51] in (d) and (e); [34] in (f); [52] in (g); [22] in (h); [35] in (i); [23, 36] (black) and [53] (purple) in (j); [37] in (k); [21, 38, 39] in (l); [16] for  $J/\psi\pi^+\pi^-$  (black) and [15] for  $J/\psi\pi^0\pi^0$  (purple, doubled) in (m); [18] for  $J/\psi K^+K^-$  (black) and [17] for  $J/\psi K_S^0 K_S^0$  (purple, doubled) in (n); [19] in (o); [20] in (p). The experimental uncertainties include statistical and systematic ones.

Long-range  $Z$ -shape  $Rc \rightarrow R'c'$  interactions couple the channels in the groups (A) and (B) but not (C). Short-range interactions (e.g.,  $\rho$ -,  $\omega$ -,  $\sigma$ -exchange) [57–59] should also exist, but their details are uncertain. Since fitting these mechanisms to data is computationally too demanding, they are assumed to be absorbed by bare  $\psi_i$  couplings and masses.

**Results.**— Our couple-channel model is fitted to  $e^+e^-$  cross section data (19 final states) as shown in Figs. 2 and 3(a). The fit also includes invariant mass and angular distribution data shown in Figs. 3(b-j) and those not shown here. The dressed  $\psi \rightarrow Rc$  vertex can be expanded into direct-decay and single-triangle terms [Fig. 1(b)], and each contribution is shown. Five bare  $\psi$  states are included to obtain the reasonable fits. In addition, we consider  $\psi(4660)$  as a BW amplitude to fit

the  $e^+e^- \rightarrow \psi'\pi^+\pi^-$  cross sections in  $\sqrt{s} > 4.6$  GeV [Fig. 2(o)]. The currently available data is insufficient to include  $\psi(4660)$  in the coupled-channel amplitude; more data in  $\sqrt{s} > 4.6$  GeV are necessary, including charm-strange final states such as  $D^{(*)}\bar{D}_s^{(*)}K$ .

The  $e^+e^- \rightarrow D_{(s)}^{(*)}\bar{D}_{(s)}^{(*)}$  data require threshold enhancements. Thus we consider moderately attractive  $D_{(s)}^{(*)}\bar{D}_{(s)}^{(*)}$  contact interactions for additional elastic final state interactions;  $D^*\bar{D} \rightarrow D\bar{D}$  term is included perturbatively to gain the  $D^*\bar{D}$  threshold enhancement for the  $D\bar{D}$  data. This enhances the blue dashed curves to red solid ones for  $e^+e^- \rightarrow D_{(s)}^{(*)}\bar{D}_{(s)}^{(*)}$  in Fig. 2.

In the present analysis with 5 bare  $\psi_i$  states and  $Rc$  channels (Table I), we have 177 fitting parameters in total from:  $m_{\psi_i}$ ; real coupling constants in  $\Gamma_{cR,\psi_i}$ ,  $\Gamma_{cR,e^+e^-}$ ,

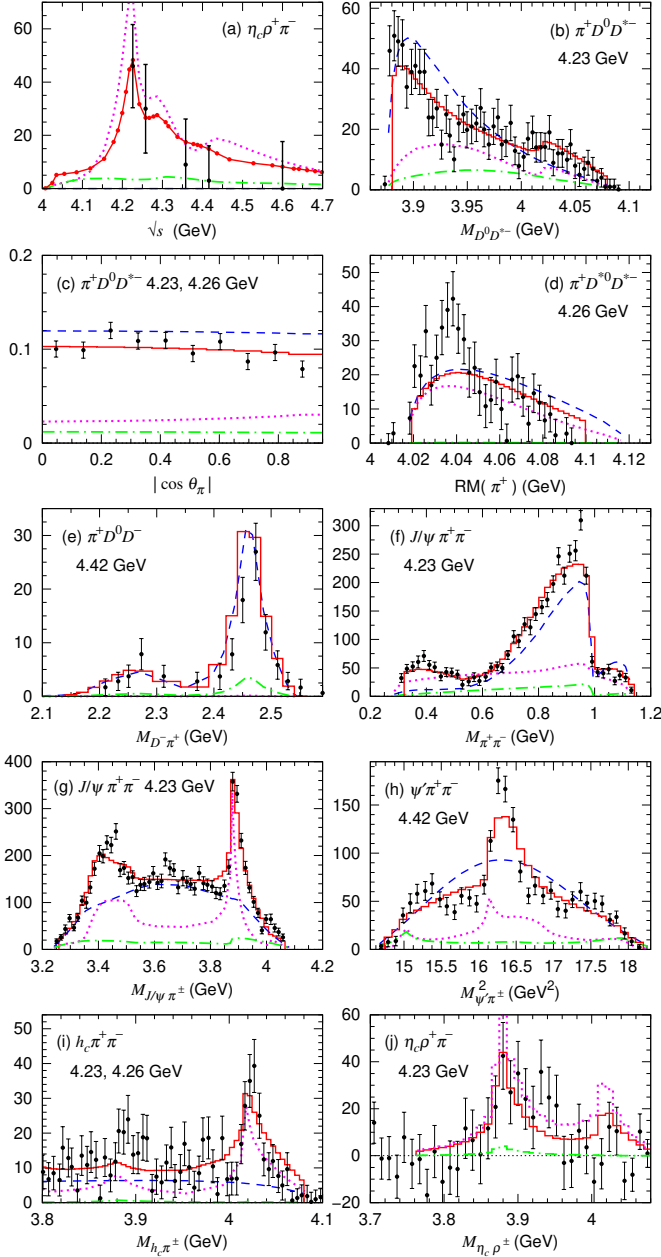


FIG. 3. (a) Continued from Fig. 2;  $\rho \rightarrow \pi\pi$  is considered. (b),(d)-(j) Selected invariant mass distributions (unit: events per bin) in  $e^+e^-$  annihilations; the final state and  $\sqrt{s}$  are indicated in each panel. (c) Angle between  $\pi$  and the beam direction in the total CM frame (unit: fractional yield). The data, from which backgrounds have been subtracted, are from [40] in (a) and (j); [41] in (b) and (c); [35] in (d); [52] in (e); [42] in (f) and (g); [25] in (h); [43] in (i). See Fig. 2 for other features.

$\Gamma_{\psi_i, e^+e^-}$ ,  $Z_c$  amplitude, and  $D_{(s)}^{(*)}\bar{D}_{(s)}^{(*)}$  contact interactions;  $\psi(4660)$  BW mass, width, and complex decay couplings to  $f_0\psi'$ . Cutoffs of dipole form factors in  $\Gamma_{cR, \psi_i}$  and  $\Gamma_{cR, e^+e^-}$  are mostly fixed to 1 GeV. However, cutoffs in  $\Gamma_{cR, e^+e^-}$  with  $Rc = D_{(s)}^{(*)}\bar{D}_{(s)}^{(*)}$  are adjusted to con-

trol the energy dependences of the NR contributions in Figs. 2(a-f).

Remarks are in order. As a consequence of the coupled-channel fit, our model creates common structures in different processes, even if not necessarily required by the data. For example,  $\psi(4040)$  peaks appear in  $D^*\bar{D}$  [Fig. 2(b)] and  $D_s\bar{D}_s$  [Fig. 2(d)] to fit the data, and they also appear in others [Fig. 2(j,m,o,p)] for which data at the peak are lacking. In Figs. 2(m,o,p), the single-triangle contributions show enhancements at  $\sqrt{s} \sim 4.28$  GeV due to the  $D_1(2420)\bar{D}$  threshold cusp enhanced by a TS. This TS-induced enhancement in  $e^+e^- \rightarrow J/\psi\pi\pi$  was attributed to  $Y(4320)$  in the experimental analyses [16, 24]. The  $J/\psi K^+K^-$  data [Fig. 2(n)] show an enhancement suggesting  $Y(4500)$  [18]. However, our model does not fit it since the data are rather fluctuating in this region, and the  $J/\psi K_S K_S$  data does not indicate the same enhancement. For  $\pi D^*\bar{D}^*$  [Fig. 2(i)], the higher energy region is not well fitted, even if a  $\psi(4660)$  BW contribution is included. Describing  $\psi(4660)$  in the coupled-channel framework might be important for a reasonable fit. The  $\pi^+$  recoil mass distribution [Fig. 3(d)] is not well fitted. However, the data extend only up to 4.09 GeV while the actual kinematical end is  $\sim 4.12$  GeV. This implies a significant efficiency correction to this line-shape.

We analytically continue the coupled-channel amplitude [60] fitted to the dataset, and find vector charmonium poles  $E_\psi$  that satisfy  $\det[\bar{G}^{-1}(E_\psi)] = 0$ ; see Eq. (6). Pole uncertainty estimates are generally difficult in global coupled-channel analyses, and simplified methods have been used [61, 62]. Here we estimate the uncertainties by introducing complex parameters  $\delta m_{\psi_i}$  as  $m_{\psi_i} \rightarrow m_{\psi_i} + \delta m_{\psi_i}$  in Eq. (6), and varying  $\delta m_{\psi_i}$  and  $\psi(4660)$  BW parameters around the default fit; see the Supplemental Material.

Seven states in Table II are found for five bare states. The bare states coupled with hadronic continuums (Table I) can generate resonances more than themselves. A similar finding is in nucleon resonances [63]. There exist two poles on the same Riemann sheet (RS) at  $M \sim 4.23$  GeV with different widths; the situation is similar at  $M \sim 4.38$  GeV. This observation hints a solution to the  $Y$ -width problem. If the two poles have different process-dependences in branching fractions, bumps at  $\sqrt{s} \sim 4.23$  and 4.38 GeV would have different widths for different processes. We will address this [45].

Compared with PDG [4],  $\psi(4040)$  width is significantly narrower, and the well-established  $\psi(4160)$  does not exist. This (also Ref. [32]) might suggest assigning  $\psi(4230)$  to the  $\psi(2D)$  quark-model state. Since the  $\psi(4040)$ ,  $\psi(4160)$ , and  $\psi(4415)$  properties in PDG are mainly from a simple BW fit to the  $R$  value [44], artifacts might happen to cause the above differences.

Finally, Table III presents the  $Z_c$  poles. The uncertainties are estimated by varying couplings in  $\gamma^* \rightarrow \psi_i$ ,



TABLE II. Vector charmonium poles ( $E_\psi$ ) and  $\psi(4660)$  BW parameters. The mass and width are  $M = \text{Re}[E_\psi]$  and  $\Gamma = -2\text{Im}[E_\psi]$ , respectively. When more than one pole exist at similar energies but on different RS, the one closest to the physical real energy is shown.

This work		PDG [4]		
$M$ (MeV)	$\Gamma$ (MeV)	$M$ (MeV)	$\Gamma$ (MeV)	
$3775 \pm 2.0$	$28 \pm 1.0$	$3778.1 \pm 0.7$	$27.5 \pm 0.9$	$\psi(3770)$
$4026 \pm 0.1$	$25 \pm 0.3$	$4039 \pm 1$	$80 \pm 10$	$\psi(4040)$
$4232 \pm 1.0$	$114 \pm 1.7$	$4191 \pm 5$	$70 \pm 10$	$\psi(4160)$
$4226 \pm 0.4$	$36 \pm 0.8$	$4222.5 \pm 2.4$	$48 \pm 8$	$\psi(4230)$
$4309 \pm 0.6$	$328 \pm 0.9$	—	—	—
$4369 \pm 0.1$	$183 \pm 0.2$	$4374 \pm 7$	$118 \pm 12$	$\psi(4360)$
$4394 \pm 0.7$	$93 \pm 0.9$	$4421 \pm 4$	$62 \pm 20$	$\psi(4415)$
$4690 \pm 7.3$	$106 \pm 8.8$	$4630 \pm 6$	$72_{-12}^{+14}$	$\psi(4660)$

TABLE III.  $J^{PC} = 1^{+-}$   $D^*\bar{D} - D^*\bar{D}^* - J/\psi\pi - \psi'\pi - h_c\pi - \eta_c\rho$  coupled-channel scattering amplitude poles. The RS,  $s_{D^*\bar{D}}, s_{D^*\bar{D}^*}$ , is specified by  $s_x = p(u)$  indicating the physical (unphysical) sheet of a channel  $x$ .

This work		PDG [4]		
$E_{\text{pole}}$ (MeV)	RS	$M$ (MeV)	$\Gamma$ (MeV)	
$(3839 \pm 11) + (20 \pm 3)i$	$up$	$3887.1 \pm 2.6$	$28.4 \pm 2.6$	$Z_c(3900)$
$(3985 \pm 7) + (28 \pm 5)i$	$pu$	$4024.1 \pm 1.9$	$13 \pm 5$	$Z_c(4020)$

$\psi_i(\gamma^*) \rightarrow D_1(2420)\bar{D}^{(*)}$ , and the  $Z_c$  amplitude. One pole (the other) is found at  $\sim 40$  MeV below the  $D^*\bar{D}$  ( $D^*\bar{D}^*$ ) threshold, on the unphysical sheets of this channels<sup>3</sup>. They are  $D^*\bar{D}$  and  $D^*\bar{D}^*$  virtual states, respectively. Our result is different from experimental [41, 42, 64] and most phenomenological analyses [65–69] that found poles near the PDG values. We make two points to support our result. First, our model has been more extensively tested by the data. While most analysis models fit the  $M_{\pi J/\psi}$  and  $M_{D^*\bar{D}}$  lineshape data where the  $Z_c(3900)$  signals are clearest, only our model also fits the cross section data that can test  $Z_c$  production mechanisms and  $Z_c$ -pole residues. The ratio  $\sigma(e^+e^- \rightarrow J/\psi\pi\pi)/\sigma(e^+e^- \rightarrow \pi D^*\bar{D})$  inherent in the other models should be confronted with the data. Second, our result is more consistent with lattice QCD results [70–74] that suggested a weak  $D^*\bar{D}$  interaction and no  $Z_c(3900)$  as a bound or narrow resonance state.

*Summary and outlook.*— We conducted a global coupled-channel analysis of most of available  $e^+e^- \rightarrow c\bar{c}$  data in  $\sqrt{s} = 3.75 - 4.7$  GeV, and obtained vector charmonium and  $Z_c$  poles. In the future, efficiency-corrected and background-free Dalitz plots should be analyzed to

fully consider the experimental constraints on the resonance properties. Such an effort has been made in the light-hadron sector [56, 75].

We acknowledge F.-K. Guo, Q. Wang, J.-J. Wu, and Z.-Y. Zhou for useful discussions. This work is in part supported by National Natural Science Foundation of China (NSFC) under contracts U2032103 and 11625523, and also by National Key Research and Development Program of China under Contracts 2020YFA0406400.

## Supplemental Material

### 1. Cross section formula

The cross section for a three meson ( $abc$ ) production from an  $e^+e^-$  annihilation ( $e^+e^- \rightarrow abc$ ) is given by

$$d\sigma_{e^+e^- \rightarrow abc} = \sum_{\bar{i}f} \mathcal{B} \frac{(2\pi)^4 \delta^{(4)}(p_i - p_f)}{4v_{\text{rel}} E_{e^+} E_{e^-}} |\mathcal{M}_{fi}|^2 (2m_e)^2 \times \frac{d^3 p_a}{(2\pi)^3 2E_a} \frac{d^3 p_b}{(2\pi)^3 2E_b} \frac{d^3 p_c}{(2\pi)^3 2E_c}, \quad (8)$$

with a Bose factor  $\mathcal{B} = 1/3!$  for three identical particles  $abc$ ,  $\mathcal{B} = 1/2!$  for identical two particles among  $abc$ , and  $\mathcal{B} = 1$  otherwise;  $\sum_{\bar{i}f}$  indicates the average (sum) of initial (final) spin states. The invariant amplitude  $\mathcal{M}_{fi}$  is related to Eqs. (1) and (2) by

$$\begin{aligned} \mathcal{M}_{fi} &= -(2\pi)^3 \sqrt{8E_{e^+} E_{e^-} E_a E_b E_c / m_e^2} \\ &\times \left( A_{abc, e^+e^-}^\psi + A_{abc, e^+e^-}^{\text{NR}} \right) \\ &= e l^\mu \tilde{\mathcal{M}}_\mu^{abc} / q^2, \end{aligned} \quad (9)$$

where the lepton current matrix element  $l^\mu (= \bar{v}_{e^+} \gamma^\mu u_{e^-})$  and the virtual photon propagator ( $1/q^2$ ) have been factored out;  $e = \sqrt{4\pi\alpha}$  and  $\alpha$  is the fine structure constant. Then, the cross section in the total center-of-mass (CM) frame can be written as:

$$d\sigma_{e^+e^- \rightarrow abc} = \sum_f \mathcal{B} \frac{\alpha}{512\pi^3 s^3} (|\tilde{\mathcal{M}}_x^{abc}|^2 + |\tilde{\mathcal{M}}_y^{abc}|^2) \times dm_{ab}^2 dm_{ac}^2 d\cos\theta_c d\bar{\phi}_a, \quad (10)$$

where the  $z$ -axis is taken along the  $e^+e^-$  beam direction;  $m_{ab}$  and  $m_{ac}$  are the invariant masses of the  $ab$  and  $ac$  subsystems, respectively;  $\sqrt{s}$  is the total energy;  $\theta_c$  is the polar angle of  $c$  in the total CM frame while  $\bar{\phi}_a$  is the azimuthal angle of  $a$  in the  $ab$  CM frame.

Similarly, a two meson ( $ab$ ) production cross section in the total CM frame is

$$\begin{aligned} d\sigma_{e^+e^- \rightarrow ab} &= \sum_{\bar{i}f} \mathcal{B} \frac{(2\pi)^4 \delta^{(4)}(p_i - p_f)}{4v_{\text{rel}} E_{e^+} E_{e^-}} |\mathcal{M}_{fi}|^2 (2m_e)^2 \\ &\times \frac{d^3 p_a}{(2\pi)^3 2E_a} \frac{d^3 p_b}{(2\pi)^3 2E_b} \\ &= \sum_f \frac{\mathcal{B} \alpha p_a}{8(\sqrt{s})^5} (|\tilde{\mathcal{M}}_x^{ab}|^2 + |\tilde{\mathcal{M}}_y^{ab}|^2) d\cos\theta_a. \end{aligned} \quad (11)$$

<sup>3</sup> Section 50 in Ref. [4] defines (un)physical sheet.

## 2. Two-meson scattering models

The amplitudes  $R = D_0^*(2300)$ ,  $f_0$ ,  $f_2$ , and  $Z_c$  in group (B) of Table I are described with two-meson scattering models, and the formulas and the  $f_0$  amplitude are presented in Appendix A of Ref. [56]. Here we present details of the  $D_0^*(2300)$ ,  $f_2$ , and  $Z_c$  amplitudes. Descriptions of the scattering models such as the number of  $R$  and contact interactions are specified in Table IV.

We make several remarks on the  $Z_c$  amplitude. By considering the heavy quark spin symmetry, we set the coupling strengths for  $D^*\bar{D} \rightarrow D^*\bar{D}$  and  $D^*\bar{D}^* \rightarrow D^*\bar{D}^*$  interactions the same [76]; the notation of  $D^*\bar{D}$  implicitly include  $\bar{D}^*D$  to form the negative  $C$ -parity state. We assume no interactions between the hidden charm channels such as  $J/\psi\pi$ ,  $\psi'\pi$ ,  $h_c\pi$ , and  $\eta_c\rho$ . For  $\eta_c\rho$  loops, we consider the  $\rho$  width ( $\Gamma_\rho$ ). Specifically, we replace the energy denominator in Eq. (A5) of Ref. [56] and use

$$E - E_{\eta_c}(q) - E_\rho(q) + i\Gamma_\rho(s_\rho)/2, \quad (12)$$

with  $s_\rho = (E - E_{\eta_c}(q))^2 - q^2$  and

$$\Gamma_\rho(s_\rho) = 2\pi g_\rho^2 \frac{p_\pi^3}{s_\rho} \frac{1}{(1 + p_\pi^2/\Lambda_\rho^2)^5} \theta(\sqrt{s_\rho} - 2m_\pi), \quad (13)$$

where  $p_\pi$  satisfies  $s_\rho = 4E_\pi^2(p_\pi)$ . The nominal value  $\Gamma_\rho((775 \text{ MeV})^2) = 150 \text{ MeV}$  is obtained with  $g_\rho = 0.75$  and  $\Lambda_\rho = 1 \text{ GeV}$ .

The coupling parameters in the two-meson scattering models are determined as follows. Our  $f_2$  amplitude is fitted to the empirical  $\pi\pi$   $d$ -wave phase shift [77]. The  $D\pi$   $s$ -wave ( $D_0^*$ ) amplitude is fitted to that based on the lattice QCD spectrum [55]. The  $Z_c$  amplitude are determined in the present global fit. Numerical values of the fitting parameters are given in Tables V–VII.

After the fits, resonance poles are extracted from the amplitudes and presented in Table VIII. The  $Z_c$  poles are presented in Table III of the main text. The  $f_2$  pole location is consistent with the PDG average [4]. The LQCD-based amplitude has a  $D_0^*$  pole at  $2105_{-8}^{+6} - i102_{-12}^{+10} \text{ MeV}$  [55], and our  $D_0^*$  pole in Table VIII is consistent.

### 3. $D^{(*)}\bar{D}^{(*)}$ and $D_s^{(*)}\bar{D}_s^{(*)}$ contact interactions

We consider  $D_{(s)}^{(*)}\bar{D}_{(s)}^{(*)}$  contact interactions to better fit the  $D_{(s)}^{(*)}\bar{D}_{(s)}^{(*)}$  cross section data with threshold enhancements. Labeling channels with  $\alpha$  and  $\beta$ , our interaction potential for an  $L$ -wave  $\alpha \rightarrow \beta$  process is given by

$$v_{\beta,\alpha}(p', p) = f_\beta^L(p') h_{\beta\alpha} f_\alpha^L(p), \quad (14)$$

where  $h_{\beta\alpha}$  is a coupling constant and  $h_{\beta\alpha} = h_{\alpha\beta}$ . The dipole form factor  $f_\alpha^L$  is given by

$$f_\alpha^L(p) = \frac{1}{\sqrt{E_{1\alpha}E_{2\alpha}}} \left( \frac{\Lambda^2}{\Lambda^2 + p^2} \right)^{2+L/2} \left( \frac{p}{m_\pi} \right)^L, \quad (15)$$

where  $E_{i\alpha}$  is the energy of a particle  $i$  in the channel  $\alpha$ ; we use  $\Lambda = 1 \text{ GeV}$  and  $L = 1$  in the present case.

We implement this rescattering effect in the dressed decay vertices  $\bar{\Gamma}_{Rc,\psi_i}$  in Eq. (4) that can be expressed by

$$\begin{aligned} \bar{\Gamma}_{cR,\psi_i}(\mathbf{p}_c, E) &= \sum_{SL,L^z} (s_c s_c^z s_R s_R^z | S s_c^z + s_R^z) \\ &\times (LL^z S s_c^z + s_R^z | 1 s_\psi^z) (t_R t_R^z t_c t_c^z | 00) \\ &\times Y_{L,L^z}(-\hat{p}_c) \bar{F}_{(cR)_{SL},\psi_i}(p_c, E), \end{aligned} \quad (16)$$

where  $Y_{LL^z}(\hat{q})$  denotes the spherical harmonics with  $\hat{q} \equiv \mathbf{q}/|\mathbf{q}|$ . The parentheses are Clebsch-Gordan coefficients, and  $t_x$  and  $t_x^z$  are the isospin of a particle  $x$  and its  $z$ -component, respectively. We introduced the dressed  $M_i^* \rightarrow Rc$  vertex function  $\bar{F}_{(cR)_{SL},\psi_i}$ . For the rescattering effect,  $\bar{F}_{\alpha,\psi_i}$  ( $\alpha = (cR)_{SL}$ ) is modified as  $\bar{F}_{\alpha,\psi_i} \rightarrow \bar{F}_{\alpha,\psi_i} + \Delta_{\alpha,\psi_i}$  with

$$\begin{aligned} \Delta_{\alpha,\psi_i} &= \sum_{\beta} f_\alpha^L(p_c) h_{\alpha\beta} \frac{1}{1 - h_{\beta\beta}\sigma_\beta(E)} \\ &\times \int dq q^2 \frac{f_\beta^L(q) \bar{F}_{\beta,\psi_i}(q, E)}{E - E_{1\beta}(q) - E_{2\beta}(q) + i\varepsilon}, \end{aligned} \quad (17)$$

and

$$\sigma_\beta(E) = \int dq q^2 \frac{[f_\beta^L(q)]^2}{E - E_{1\beta}(q) - E_{2\beta}(q) + i\varepsilon}. \quad (18)$$

The nonresonant dressed decay vertices  $\bar{\Gamma}_{Rc,e^+e^-}$  discussed above Eq. (5) are also modified in a similar manner.

Some specifications to Eq. (14) are as follows. For fitting the  $D\bar{D}$  final state, the  $D^*\bar{D}$  threshold enhancement is needed. We thus consider the  $D^*\bar{D}$  rescattering followed by a perturbative transition to  $D\bar{D}$ . For the other  $D_{(s)}^{(*)}\bar{D}_{(s)}^{(*)}$  final states, we consider the elastic rescattering. Table IX lists nonzero  $h_{\alpha\beta}$  values determined by the global fit. The interactions are moderately attractive, and do not create resonance poles. We do not include the interactions of Eq. (14) in the self energy of Eq. (7) for not increasing the computation time. We just confirmed this contribution to be small by inserting  $h_{\beta\beta}\tau_{R\beta,R'}/(1 - h_{\beta\beta}\sigma_\beta(E))$  in Eq. (7) once.

## 4. Uncertainty of vector charmonium poles

In a standard procedure of estimating uncertainties of (resonance) pole values, all fitting parameters are varied around the minimum  $\chi^2$  to generate an error matrix of the parameters, and then the matrix is used for the error propagation to the pole values. In our global coupled-channel analysis, however, this procedure is practically impossible. This is because the cross section calculation is rather time-consuming for the four-dimensional phase-space integral in Eq. (10), and we have too many

TABLE IV. Description of two-meson scattering models. Partial waves are specified by the orbital angular momentum  $L$  and the isospin  $I$ ;  $J^{PC}$  is used for  $R = Z_c$ .

$R$	$\{L, I\}$	# of bare states	channels in contact interaction	$R$ -decay channels	# of poles
$f_2$	$\{2, 0\}$	1	-	$\pi\pi, K\bar{K}$	1
$D_0^*(2300)$	$\{0, 1/2\}$	1	$D\pi$	$D\pi$	1

$R$	$I, J^{PC}$	# of bare states	channels in contact interaction	$R$ -decay channels	# of poles
$Z_c$	$1, 1^{+-}$	0	$D^*\bar{D}, D^*\bar{D}^*, J/\psi\pi, \psi'\pi, h_c\pi, \eta_c\rho$	-	2

TABLE V. Parameter values for the  $\pi\pi$  partial wave scattering model. The  $i$ -th bare  $R$  states ( $R_i$ ) has a mass of  $m_{R_i}$ , and it decays into  $h_1$  and  $h_2$  particles with couplings ( $g_{h_1 h_2, R_i}$ ) and cutoffs ( $c_{h_1 h_2, R_i}$ ). Couplings and cutoffs for contact interactions are denoted by  $h_{h_1 h_2, h_1 h_2}$  and  $b_{h_1 h_2}$ , respectively. The parameters have been defined in Appendix A of Ref. [56]. For simplicity, we suppress the superscripts,  $LI$ , of the parameters. The mass and cutoff values are given in the unit of MeV, and the couplings are dimensionless.

$R \{L, I\}$	$f_2 \{2, 0\}$
$m_{R_1}$	1500
$g_{\pi\pi, R_1}$	-0.313
$c_{\pi\pi, R_1}$	1219
$g_{K\bar{K}, R_1}$	0.179
$c_{K\bar{K}, R_1}$	1546

TABLE VI. Parameter values for the  $D\pi$  partial wave scattering model. See Table V for the description.

$R \{L, I\}$	$D_0^* \{0, 1/2\}$
$m_{R_1}$	2285
$g_{D\pi, R_1}$	8.61
$c_{D\pi, R_1}$	1000
$h_{D\pi, D\pi}$	1.38
$b_{D\pi}$	1000

TABLE VII. Parameter values for the  $Z_c$  amplitude model. The cutoff is  $b_x = 1000$  MeV for all channels  $x$ . See Table V for the description.

$R I J^{PC}$	$Z_c 11^{+-}$
$h_{D^*\bar{D}, D^*\bar{D}}$	-1.00
$h_{D^*\bar{D}, D^*\bar{D}^*}$	-0.90
$h_{D^*\bar{D}, J/\psi\pi}$	-1.10
$h_{D^*\bar{D}, \psi'\pi}$	0.98
$h_{D^*\bar{D}, h_c\pi}$	0.17
$h_{D^*\bar{D}, \eta_c\rho}$	-1.55
$h_{D^*\bar{D}^*, D^*\bar{D}^*}$	-1.00
$h_{D^*\bar{D}^*, J/\psi\pi}$	-0.45
$h_{D^*\bar{D}^*, \psi'\pi}$	0.89
$h_{D^*\bar{D}^*, h_c\pi}$	0.47
$h_{D^*\bar{D}^*, \eta_c\rho}$	1.13

TABLE VIII. Pole positions ( $M_{\text{pole}}$ ) in our  $\pi\pi$  and  $D\pi$  scattering amplitudes. The Riemann sheets (RS) of the pole positions are specified by  $(s_{\pi\pi}, s_{K\bar{K}})$  for  $\pi\pi$  and  $(s_{D\pi})$  for  $D\pi$ ;  $s_x = p(u)$  indicates that a pole is on the physical (unphysical) sheet of the channel  $x$ .

$\{L, I\}$	$M_{\text{pole}}$ (MeV)	RS	name
$\{2, 0\}$	$1249 - 102i$	$(uu)$	$f_2(1270)$
$\{0, 1/2\}$	$2104 - 100i$	$(u)$	$D_0^*(2300)$

TABLE IX. Parameter values for  $h_{\beta\alpha}$  in Eq. (14).

$h_{D\bar{D}, D^*\bar{D}}$	0.049
$h_{D^*\bar{D}, D^*\bar{D}}$	-0.120
$h_{D^*\bar{D}^*, D^*\bar{D}^*}$	-0.144
$h_{D_s\bar{D}_s, D_s\bar{D}_s}$	-0.172
$h_{D_s^*\bar{D}_s, D_s^*\bar{D}_s}$	-0.181
$h_{D_s^*\bar{D}_s^*, D_s^*\bar{D}_s^*}$	-0.181

177 fitting parameters to reach a convergence in the  $\chi^2$ -minimization. This problem is also common in global coupled-channel analyses for nucleon resonances [61, 62].

We thus use a practical uncertainty estimation method hinted by Ref. [61]. We first adjust 177 fitting parameters in the model described in the main text, and obtain a default fit to the data shown in Figs. 2 and 3. The fit includes more invariant mass distributions in the references listed in the Fig. 3 caption. Then, we introduce complex parameters  $\delta m_{\psi_i}$  in Eq. (6) as

$$m_{\psi_i} \rightarrow m_{\psi_i} + \delta m_{\psi_i}. \quad (19)$$

We then refit the data by varying  $\delta m_{\psi_i}$  and  $\psi(4660)$  BW parameters to obtain an error matrix; the other 175 fitting parameters are fixed to the default values. The error matrix is used to estimate the vector charmonium pole uncertainties in Table II through the standard error propagation. We note that the pole values from the default fit (shown in Table II) and those obtained after fitting  $\delta m_{\psi_i}$  are slightly different; two reasons: (i) The

imaginary parts of  $\delta m_{\psi_i}$  are degrees of freedom not existent in the original model. (ii) Some data points are additionally weighted in the default fit so that the fit is overall reasonable; without the weights, data points with large errors are not reasonably fitted. The purpose of this error analysis is to estimate how much the pole values can fluctuate due to the experimental errors. Thus, in Table II, we list the pole values from the default fit and their uncertainties are from the above uncertainty analysis.

### 5. Uncertainty estimation of $Z_c$ poles

We estimate uncertainties of the  $Z_c$  poles as below. We select parameters that are presumably most relevant to the  $Z_c$  poles, and vary them around the default values to obtain an error matrix; the other parameters are fixed at their default-fit values. Then the error matrix is used to estimate uncertainties of  $Z_c$  poles through the standard error propagation. We consider two cases for selecting the parameters: (i) 10 fitting parameters in the  $Z_c$  amplitude in Table VII ( $h_{D^*\bar{D},D^*\bar{D}} = h_{D^*\bar{D}^*,D^*\bar{D}^*}$ ); (ii) 24 fitting parameters in the  $Z_c$  amplitude,  $\Gamma_{\psi_i,e^+e^-}$ ,  $\Gamma_{cR,\psi_i}$ , and  $\Gamma_{cR,e^+e^-}$  ( $Rc = D_1(2420)\bar{D}^{(*)}$  only). We do not find a significant difference between (i) and (ii) in the  $Z_c$  pole uncertainties, and we list those from (ii) in Table III. The pole values in Table III are from the default fit for the reason discussed in the above section 3.

---

\* satoshi@sdu.edu.cn

- [1] B. Aubert et al. (BABAR Collaboration), Observation of a broad structure in the  $\pi^+\pi^-J/\psi$  Mass Spectrum around 4.26 GeV/ $c^2$ , Phys. Rev. Lett. **95**, 142001 (2005).
- [2] T.E. Coan et al. (CLEO Collaboration), Charmonium Decays of  $Y(4260)$ ,  $\psi(4160)$ , and  $\psi(4040)$ , Phys. Rev. Lett. **96**, 162003 (2006).
- [3] C.Z. Yuan et al. (Belle Collaboration), Measurement of the  $e^+e^- \rightarrow \pi^+\pi^-J/\psi$  Cross Section Via Initial-State Radiation at Belle, Phys. Rev. Lett. **99**, 182004 (2007).
- [4] R.L. Workman et al. (Particle Data Group), Review of Particle Physics, Prog. Theor. Exp. Phys. **2022**, 083C01 (2022).
- [5] B. Aubert et al. (BABAR Collaboration), Evidence of a Broad Structure at an Invariant Mass of 4.32 GeV/ $c^2$  in the Reaction  $e^+e^- \rightarrow \pi^+\pi^-\psi(2S)$  Measured at BABAR, Phys. Rev. Lett. **98**, 212001 (2007).
- [6] X. L. Wang et al. (Belle Collaboration), Observation of Two Resonant Structures in  $e^+e^- \rightarrow \pi^+\pi^-\psi(2S)$  via Initial-State Radiation at Belle, Phys. Rev. Lett. **99**, 142002 (2007).
- [7] H.-X. Chen, W. Chen, X. Liu, and S.-L. Zhu, The hidden-charm pentaquark and tetraquark states, Phys. Rep. **639**, 1 (2016).
- [8] A. Hosaka, T. Iijima, K. Miyabayashi, Y. Sakai, and S. Yasui, Exotic hadrons with heavy flavors:  $X$ ,  $Y$ ,  $Z$ , and related states, PTEP **2016**, 062C01 (2016).
- [9] R.F. Lebed, R.E. Mitchell, and E.S. Swanson, Heavy-Quark QCD Exotica, Prog. Part. Nucl. Phys. **93**, 143 (2017).
- [10] A. Esposito, A. Pilloni, and A.D. Polosa, Multiquark Resonances, Phys. Rept. **668**, 1 (2017).
- [11] A. Ali, J.S. Lange, and S. Stone, Exotics: Heavy Pentaquarks and Tetraquarks, Prog. Part. Nucl. Phys. **97**, 123 (2017).
- [12] F.-K. Guo, C. Hanhart, U.-G. Meißner, Q. Wang, Q. Zhao, and B.-S. Zou, Hadronic molecules, Rev. Mod. Phys. **90**, 015004 (2018).
- [13] S.L. Olsen, T. Skwarnicki, and D. Zieminska, Nonstandard heavy mesons and baryons: Experimental evidence, Rev. Mod. Phys. **90**, 015003 (2018).
- [14] N. Brambilla, S. Eidelman, C. Hanhart, A. Nefediev, C.-P. Shen, C.E. Thomas, A. Vairo, and C.-Z. Yuan, The  $XYZ$  states: Experimental and theoretical status and perspectives, Phys. Rept. **873**, 1 (2020).
- [15] M. Ablikim et al. (BESIII Collaboration), Study of the process  $e^+e^- \rightarrow \pi^0\pi^0J/\psi$  and neutral charmoniumlike state  $Z_c(3900)^0$ , Phys. Rev. D **102**, 012009 (2020).
- [16] M. Ablikim et al. (BESIII Collaboration), Study of the resonance structures in the process  $e^+e^- \rightarrow \pi^+\pi^-J/\psi$ , Phys. Rev. D **106**, 072001 (2022).
- [17] M. Ablikim et al. (BESIII Collaboration), Observation of the  $Y(4230)$  and evidence for a new vector charmoniumlike state  $Y(4710)$  in  $e^+e^- \rightarrow K_S^0K_S^0J/\psi$ , Phys. Rev. D **107**, 092005 (2023).
- [18] M. Ablikim et al. (BESIII Collaboration), Observation of the  $Y(4230)$  and a new structure in  $e^+e^- \rightarrow K^+K^-J/\psi$ , Chin. Phys. C **46**, 111002 (2022).
- [19] M. Ablikim et al. (BESIII Collaboration), Cross section measurement of  $e^+e^- \rightarrow \pi^+\pi^-\psi(3686)$  from  $\sqrt{s} = 4.0076$  GeV to 4.6984 GeV, Phys. Rev. D **104**, 052012 (2021).
- [20] M. Ablikim et al. (BESIII Collaboration), Evidence of Two Resonant Structures in  $e^+e^- \rightarrow \pi^+\pi^-h_c$ , Phys. Rev. Lett. **118**, 092002 (2017).
- [21] M. Ablikim et al. (BESIII Collaboration), Cross section measurements of  $e^+e^- \rightarrow \omega\chi_{c0}$  from  $\sqrt{s} = 4.178$  to 4.278 GeV, Phys. Rev. D **99**, 091103(R) (2019).
- [22] M. Ablikim et al. (BESIII Collaboration), Evidence of a Resonant Structure in the  $e^+e^- \rightarrow \pi^+D^0D^{*-}$  Cross Section between 4.05 and 4.60 GeV, Phys. Rev. Lett. **122**, 102002 (2019).
- [23] M. Ablikim et al. (BESIII Collaboration), Measurement of  $e^+e^- \rightarrow \eta J/\psi$  Cross Section from  $\sqrt{s} = 3.808$  to 4.951 GeV, arXiv:2310.03361.
- [24] M. Ablikim et al. (BESIII Collaboration), Precise Measurement of the  $e^+e^- \rightarrow \pi^+\pi^-J/\psi$  Cross Section at Center-of-Mass Energies from 3.77 to 4.60 GeV, Phys. Rev. Lett. **118**, 092001 (2017).
- [25] M. Ablikim et al. (BESIII Collaboration), Measurement of  $e^+e^- \rightarrow \pi^+\pi^-\psi(3686)$  from 4.008 to 4.600 GeV and observation of a charged structure in the  $\pi^\pm\psi(3686)$  mass spectrum, Phys. Rev. D **96**, 032004 (2017).
- [26] M. Ablikim et al. (BESIII Collaboration), Observation of a Charged Charmoniumlike Structure in  $e^+e^- \rightarrow \pi^+\pi^-J/\psi$  at  $\sqrt{s} = 4.26$  GeV, Phys. Rev. Lett. **110**, 252001 (2013).
- [27] Z.Q. Liu et al. (Belle Collaboration), Study of  $e^+e^- \rightarrow \pi^+\pi^-J/\psi$  and Observation of a Charged Charmoniumlike State at Belle, Phys. Rev. Lett. **110**, 252002 (2013).
- [28] M. Ablikim et al. (BESIII Collaboration), Observation



- of a Charged Charmoniumlike Structure  $Z_c(4020)$  and Search for the  $Z_c(3900)$  in  $e^+e^- \rightarrow \pi^+\pi^-h_c$ , Phys. Rev. Lett. **111**, 242001 (2013).
- [29] M. Cleven, Q. Wang, F.-K. Guo, C. Hanhart, U.-G. Meißner, and Q. Zhao,  $Y(4260)$  as the first  $S$ -wave open charm vector molecular state? Phys. Rev. D **90**, 074039 (2014).
- [30] L. von Detten, C. Hanhart, and V. Baru, The  $Y(4230)$  as a  $D_1\bar{D}$  molecule, arXiv:2309.11970.
- [31] D.-Y. Chen, X. Liu, and T. Matsuki, Interference effect as resonance killer of newly observed charmoniumlike states  $Y(4320)$  and  $Y(4390)$ , Eur. Phys. J. C **78**, (2018) 136.
- [32] Z.-Y. Zhou, C.-Y. Li, and Z. Xiao, A new look at  $\psi(4160)$  and  $\psi(4230)$ , arXiv:2304.07052.
- [33] The BESIII Collaboration, Cross section measurements of the  $e^+e^- \rightarrow D^{*+}D^{*-}$  and  $e^+e^- \rightarrow D^{*+}D^-$  processes at center-of-mass energies from 4.085 to 4.600 GeV, J. High Energy Phys. 05 (2022) 155.
- [34] M. Ablikim et al. (BESIII Collaboration), Precise Measurement of the  $e^+e^- \rightarrow D_s^{*+}D_s^{*-}$  Cross Sections at Center-of-Mass Energies from Threshold to 4.95 GeV, Phys. Rev. Lett. **131**, 151903 (2023).
- [35] M. Ablikim et al. (BESIII Collaboration), Observation of a Charged Charmoniumlike Structure in  $e^+e^- \rightarrow (D^*\bar{D}^*)^\pm\pi^\mp$  at  $\sqrt{s} = 4.26$  GeV, Phys. Rev. Lett. **112**, 132001 (2014).
- [36] BESIII Collaboration, Observation of  $\psi(3770) \rightarrow \eta J/\psi$ , Phys. Rev. D **107**, L091101 (2023).
- [37] M. Ablikim et al. (BESIII Collaboration), Cross section measurement of  $e^+e^- \rightarrow \eta' J/\psi$  from  $\sqrt{s} = 4.178$  to 4.600 GeV, Phys. Rev. D **101**, 012008 (2020).
- [38] M. Ablikim et al. (BESIII Collaboration), Study of  $e^+e^- \rightarrow \omega\chi_{cJ}$  at Center of Mass Energies from 4.21 to 4.42 GeV, Phys. Rev. Lett. **114**, 092003 (2015).
- [39] M. Ablikim et al. (BESIII Collaboration), Observation of  $e^+e^- \rightarrow \omega\chi_{c1,2}$  near  $\sqrt{s} = 4.42$  and 4.6 GeV, Phys. Rev. D **93**, 011102(R) (2016).
- [40] M. Ablikim et al. (BESIII Collaboration), Study of  $e^+e^- \rightarrow \pi^+\pi^-\pi^0\eta_c$  and evidence for  $Z_c(3900)^\pm$  decaying into  $\rho^\pm\eta_c$ , Phys. Rev. D **100**, 111102(R) (2019).
- [41] M. Ablikim et al. (BESIII Collaboration), Confirmation of a charged charmoniumlike state  $Z_c(3885)^\mp$  in  $e^+e^- \rightarrow \pi^\pm(D\bar{D}^*)^\mp$  with double  $D$  tag, Phys. Rev. D **92**, 092006 (2015).
- [42] M. Ablikim et al. (BESIII Collaboration), Determination of the Spin and Parity of the  $Z_c(3900)$ , Phys. Rev. Lett. **119**, 072001 (2017).
- [43] M. Ablikim et al. (BESIII Collaboration), Observation of a Charged Charmoniumlike Structure  $Z_c(4020)$  and Search for the  $Z_c(3900)$  in  $e^+e^- \rightarrow \pi^+\pi^-h_c$ , Phys. Rev. Lett. **111**, 242001 (2013).
- [44] M. Ablikim et al. (BES Collaboration), Determination of the  $\psi(3770)$ ,  $\psi(4040)$ ,  $\psi(4160)$  and  $\psi(4415)$  resonance parameters, Phys. Lett. B **660**, 315 (2008).
- [45] S.X. Nakamura, X.-H. Li, H.-P. Peng, Z.-T. Sun, and X.-R. Zhou, in preparation.
- [46] H. Kamano, S.X. Nakamura, T.-S.H. Lee, and T. Sato, Unitary coupled-channels model for three-mesons decays of heavy mesons, Phys. Rev. D **84**, 114019 (2011).
- [47] S.X. Nakamura, H. Kamano, T.-S.H. Lee, and T. Sato, Extraction of meson resonances from three-pions photoproduction reactions, Phys. Rev. D **86**, 114012 (2012).
- [48] S.X. Nakamura, Coupled-channel analysis of  $D^+ \rightarrow K^-\pi^+\pi^+$  decay, Phys. Rev. D **93**, 014005 (2016).
- [49] G. Pakhlova et al. (Belle Collaboration), Measurement of the near-threshold  $e^+e^- \rightarrow D\bar{D}$  cross section using initial-state radiation, Phys. Rev. D **77**, 011103(R) (2008).
- [50] V. Zhukova et al. (Belle Collaboration), Angular analysis of the  $e^+e^- \rightarrow D^{(*)\pm}D^{*\mp}$  process near the open charm threshold using initial-state radiation, Phys. Rev. D **97**, 012002 (2018).
- [51] G. Pakhlova et al. (Belle Collaboration), Measurement of  $e^+e^- \rightarrow D_s^{(*)+}D_s^{(*)-}$  cross sections near threshold using initial-state radiation, Phys. Rev. D **83**, 011101(R) (2011).
- [52] G. Pakhlova et al. (Belle Collaboration), Observation of the  $\psi(4415) \rightarrow D\bar{D}_2^*(2460)$  Decay Using Initial-State Radiation, Phys. Rev. Lett. **100**, 062001 (2008).
- [53] X.L.Wang et al. (Belle Collaboration), Observation of  $\psi(4040)$  and  $\psi(4160)$  decay into  $\eta J/\psi$ , Phys. Rev. D **87**, 051101(R) (2013).
- [54] P. del Amo Sanchez et al. (BABAR Collaboration), Observation of new resonances decaying to  $D\pi$  and  $D^*\pi$  in inclusive  $e^+e^-$  collisions near  $\sqrt{s} = 10.58$  GeV, Phys. Rev. D **82**, 111101(R) (2010).
- [55] M. Albaladejo, P. Fernandez-Soler, F.-K. Guo, and J. Nieves, Two-pole structure of the  $D_0^*(2400)$ , Phys. Lett. B **767**, 465 (2017).
- [56] S.X. Nakamura, Q. Huang, J.-J. Wu, H.-P. Peng, Y. Zhang, and Y.-C. Zhu, Three-body unitary coupled-channel approach to radiative  $J/\psi$  decays and  $\eta(1405/1475)$ , Phys. Rev. D **109**, 014021 (2024).
- [57] G.-J. Ding, Are  $Y(4260)$  and  $Z_2^+(4250)$   $D_1D$  or  $D_0D^*$  hadronic molecules? Phys. Rev. D **79**, 014001 (2009).
- [58] X.-K. Dong, Y.-H. Lin, and B.-S. Zou, Prediction of an exotic state around 4240 MeV with  $J^{PC} = 1^{-+}$  as the  $C$ -parity partner of  $Y(4260)$  in a molecular picture, Phys. Rev. D **101**, 076003 (2020).
- [59] X.-K. Dong, F.-K. Guo, and B.-S. Zou, A survey of heavy-antiheavy hadronic molecules, Progr. Phys. **41**, 65 (2021).
- [60] D. Sadasivan, A. Alexandru, H. Akdag, F. Amorim, R. Brett, C. Culver, M. Döring, F.X. Lee, and M. Mai, Pole position of the  $a_1(1260)$  resonance in a three-body unitary framework, Phys. Rev. D **105**, 054020 (2022).
- [61] H. Kamano, S.X. Nakamura, T.-S.H. Lee, and T. Sato, Dynamical coupled-channels model of  $K^-p$  reactions. II. Extraction of  $\Lambda^*$  and  $\Sigma^*$  hyperon resonances, Phys. Rev. C **92**, 025205 (2015).
- [62] D. Rönchen, M. Döring, U.-G. Meißner, and C.-W. Shen, Light baryon resonances from a coupled-channel study including  $K\Sigma$  photoproduction, Eur. Phys. J. A **58**, 229 (2022).
- [63] N. Suzuki, B. Juliá-Díaz, H. Kamano, T.-S.H. Lee, A. Matsuyama, and T. Sato, Disentangling the Dynamical Origin of  $P_{11}$  Nucleon Resonances, Phys. Rev. Lett. **104**, 042302 (2010).
- [64] Z.Q. Liu et al. (Belle Collaboration), Study of  $e^+e^- \rightarrow \pi^+\pi^-J/\psi$  and Observation of a Charged Charmoniumlike State at Belle, Phys. Rev. Lett. **110**, 252002 (2013).
- [65] M. Albaladejo, F.-K. Guo, C. Hidalgo-Duque, and J. Nieves,  $Z_c(3900)$ : What has been really seen?, Phys. Lett. B **755**, 337 (2016).
- [66] A. Pilloni, C. Fernandez-Ramirez, A. Jackura, V. Mathieu, M. Mikhasenko, J. Nys, and A. P. Szczepaniak, Amplitude analysis and the nature of the  $Z_c(3900)$ , Phys.

- Lett. B **772**, 200 (2017).
- [67] J. He and D.-Y. Chen,  $Z_c(3900)/Z_c(3885)$  as a virtual state from  $\pi J/\psi - \bar{D}^* D$  interaction, Eur. Phys. J. C **78**, 94 (2018).
- [68] M.-L. Du, M. Albaladejo, F.-K. Guo, and J. Nieves, Combined analysis of the  $Z_c(3900)$  and the  $Z_{cs}(3985)$  exotic states, Phys. Rev. D **105**, 074018 (2022).
- [69] Precise determination of the pole position of the exotic  $Z_c(3900)$ , Y.-H. Chen, M.-L. Du, and F.-K. Guo, arXiv:2310.15965.
- [70] S. Prelovsek and L. Leskovec, Search for  $Z_c^+(3900)$  in the  $1^{+-}$  channel on the lattice, Phys. Lett. **B727**, 172 (2013).
- [71] Y. Chen, M. Gong, Y.-H. Lei, N. Li, J. Liang, C. Liu et al., Low-energy scattering of the  $(D\bar{D}^*)^\pm$  system and the resonance-like structure  $Z_c(3900)$ , Phys. Rev. D **89**, 094506 (2014).
- [72] S. Prelovsek, C.B. Lang, L. Leskovec, and D. Mohler, Study of the  $Z_c^+$  channel using lattice QCD, Phys. Rev. D **91**, 014504 (2015).
- [73] Y. Ikeda, S. Aoki, T. Doi, S. Gongyo, T. Hatsuda, T. Inoue, T. Iritani, N. Ishii, K. Murano, and K. Sasaki, Fate of the Tetraquark Candidate  $Z_c(3900)$  from Lattice QCD, Phys. Rev. Lett. **117**, 242001 (2016).
- [74] G.K.C. Cheung, C.E. Thomas, J.J. Dudek, and R.G. Edwards, Tetraquark operators in lattice QCD and exotic flavour states in the charm sector, JHEP **11**, 033 (2017).
- [75] S.X. Nakamura, Q. Huang, J.-J. Wu, H.-P. Peng, Y. Zhang, and Y.-C. Zhu, Three-Body Unitary Coupled-Channel Analysis on  $\eta(1405/1475)$ , Phys. Rev. D **107**, L091505 (2023).
- [76] M.-L. Du, M. Albaladejo, F.-K. Guo, and J. Nieves, Combined analysis of the  $Z_c(3900)$  and the  $Z_{cs}(3985)$  exotic states, Phys. Rev. D **105**, 074018 (2022).
- [77] B. Hyams et al.,  $\pi\pi$  Phase-shift analysis from 600 to 1900 MeV, Nucl. Phys. B **64**, 134 (1973).